Journal of Sound and Vibration (1997) **207**(5), 671–691

COMPRESSION LOAD TRANSMISSION IN SCREW COMPRESSORS

G. P. Adams and Z. H. Qin

Department of Mechanical Engineering, University of Arkansas, Fayetteville, AR, U.S.A.

(*Received* 13 *December* 1996, *and in final form* 19 *May* 1997)

In the current investigations of the bearing forces in screw compressors, the supports at the bearings are basically treated as ideal, simply supported boundary conditions. By using statics theory, the loads on the rotors are converted to the bearings at the suction and discharge ends. Some studies on rotor dynamics have shown that the behaviors of a rotor bearing system are, to some extent, controlled by the bearings that support the rotor. Therefore, it is important to study the dynamic performance of the rotor bearing system in screw compressors so that the bearing forces can be more accurately described. In this paper, a numerical method is presented for computing the compression loads by integrating the pressure over the rotor surface. Vector calculus and numerical integration methods are implemented to calculate the compression loads in order to obtain a robust procedure that can be applied to arbitrary rotor profiles. In addition, a dynamic model of a rigid compressor rotor supported by two cylindrical roller bearings and a four point contact ball bearing is developed from basic principles. This model simulates the dynamic responses of a typical screw compressor configuration. It includes five degrees of freedom of rotor motion interacting with the bearings of non-linear characteristics. Under the compression loads, the resulting bearing forces in the screw compressor are compared with those obtained by assuming ideal, simply supported boundary conditions at the bearings. It is shown that the interactions betweeen the rotor and bearings are quite different by coupling the global rotor motion with the local dynamics of the bearings.

1. INTRODUCTION

Screw compressors have been widely used in gas and refrigeration industries. One of the major advantages of the screw compressor is its flexibility in performing under various operating conditions. The bearing loads in screw compressors vary with operating conditions. A method for computing the bearing loads under various operating conditions for different rotor profiles will be useful in helping designers analyze the load response of potential designs.

A recent study [1] has shown that, in a screw compressor, the compression loads dominate the bearing forces as compared to the contact forces between the rotors. Therefore, an accurate computation of compression loads is required to determine the bearing loads. The simplest way to compute the compression loads is to utilize assumptions to simplify the complex rotor profile geometry [2]. Since the compression loads depend mainly on the rotor profile geometry and pressures at the suction and discharge ends, this simplification affects the magnitudes of the computed compression loads. You *et al*. [3] presented a model to compute the bearing loads. This method divides the rotor into elements along the rotation axis, analyzes the forces on each element and numerically integrates the forces on each element to obtain the bearing loads. Typical results of bearing loads are presented as a function of rotation angle of the male rotor. Adams and Soedel

0022–460X/97/450671 + 21 $25.00/0/sv971172

[4] developed a general solution for compression load calculation based on the rotor profile geometry and pressures at the suction and discharge ends by mapping the 3D rotor surface into a 2D region. Inaccuracies in this model were associated with a straight line approximation for the interlobe seal geometry. An improvement to the compression loads model [5] uses the actual interlobe seal geometry so that the inaccuracy associated with the straight line approximation is avoided. Also, it provided an integrated formula for the computation of compression loads based on the geometry profile, seal data and pressures at suction and discharge ends.

In order to obtain the bearing loads, the compression loads on the rotors have to be transferred to the bearings. Current models for the bearing load computation describe the bearings as having ideal, simply supported boundary conditions [3, 5, 6]. By using statics theory, the loads on the rotors are transferred to the bearings at the suction and discharge ends. Some studies on the rotor dynamics have shown that the behaviors of a rotor bearing system are, to some extent, controlled by the bearings that support the rotor. Therefore, it is important to study the dynamic performance of the rotor bearing system in screw compressors so that the bearing forces can be more accurately described.

Considerable research has been accomplished in developing models to investigate the dynamic behavior of rotors and bearings. Regarding bearing modelling, Jones [7] provided analytical models for elastically constrained ball and radial roller bearings. These models define the loading and attitude of each rolling element in each bearing of the system as well as the displacement of each inner race with respect to its outer race. The author gives a complete general solution for the elastic compliances of a system of any number of ball and radial roller bearings. This work provides a fundamental theory for the later studies on the dynamic analysis of rolling bearing systems. When modelling a rotor bearing system, the bearings are sometimes described as having ideal, simply supported or clamped boundary conditions [8, 9]. In other work, the bearings are treated as purely translating springs with constant stiffness coefficients [10–12]. More recent models for the rotor bearing systems incorporate the rotor motion with bearing stiffness having non-linear characteristics [13–15]. While these studies presented valuable information, the behavior of load transmission in a screw compressor was not discussed.

In this paper, a numerical method, based on the study by Adams and Soedel [5], is presented for computing the compression loads by integrating the pressure over the rotor surface. Vector calculus and numerical integration methods are implemented to calculate the compression loads resulting in a robust procedure that can be applied to arbitrary rotor profiles. To obtain the bearing forces, a dynamic model of a rigid compressor rotor supported by two cylindrical roller bearings and a four point contact ball bearing is developed from basic principles. This model simulates a typical screw compressor configuration. It includes five degrees of freedom of rotor motion interacting with bearings of non-linear characteristics. Under the compression loads, the resulting bearing forces are compared with the bearing forces obtained by assuming ideal, simply supported boundary conditions at the bearings. It is shown that the interactions between the rotor and bearings are quite different by coupling the global rotor motion with the local dynamics of the bearings.

2. COMPRESSION LOAD COMPUTATION

A typical set of screw compressor rotors is shown in Figure 1. When the compressor is operating, the contact between the male and female rotors forms an interlobe seal curve

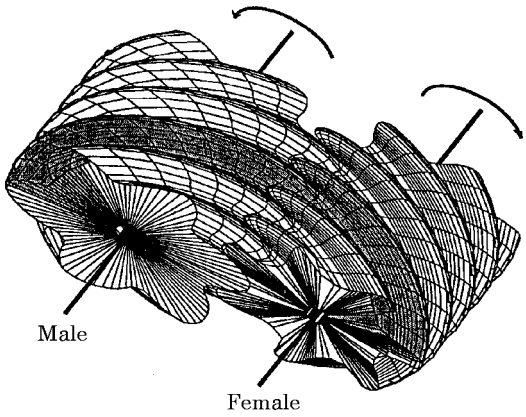

Figure 1. A typical set of screw compressor rotors.

along the male rotor. This interlobe seal curve further divides the helical sections of the male rotor into separate chambers. A suction chamber forms between the suction plane and the seal, and a compression chamber forms between the seal and the discharge plane. As the male rotor rotates, the interlobe seal for a specific section translates along the rotor axis from the suction plane to the discharge plane. The resulting decrease in the compression chamber volume causes compression of the enclosed gas. The compression loads are computed by integrating the pressure over each individual chamber and summing the results. Due to the symmetry of the rotors, the compression cycle is a periodic function of the rotation angle of the male rotor, θ_m. Therefore, the compression loads are computed for values of θ_m from 0·0 to $2\pi/N_m$. The pressure due to compression is a scalar which can be integrated over the 3D surface of the rotor. Each 3D surface S of a compression chamber is mapped into a 2D region D. The compression loads are obtained by integrating the chamber pressure over this region.

The graphical representation of the mapping scheme is shown in Figure 2. According to Adams and Soedel [5], the force due to compression is computed as

$$\mathbf{F} = \iint P \| \mathbf{T}_\phi \times \mathbf{T}_\theta \| \, \mathrm{d}\phi \, \mathrm{d}\theta = P \iint \| \mathbf{T}_\phi \times \mathbf{T}_\theta \| \, \mathrm{d}\phi \, \mathrm{d}\theta, \tag{1}$$

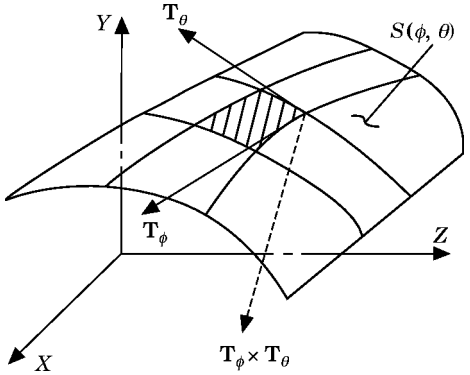

Figure 2. Mapping 3D surface into 2D region.

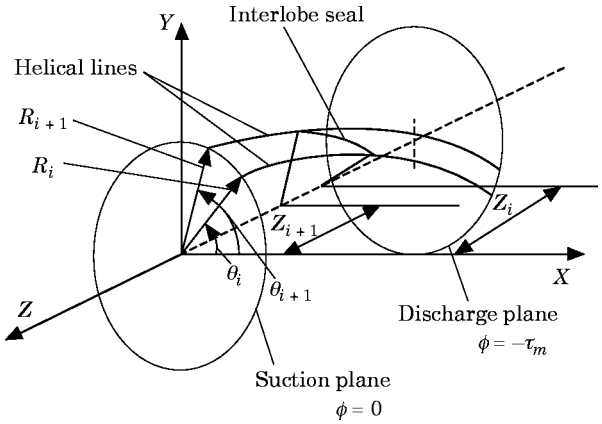

Figure 3. Co-ordinate system illustration.

where

$$\mathbf{T}_\theta = (\partial x/\partial\theta)(\phi, \theta)i + (\partial y/\partial\theta)(\phi, \theta)j + (\partial z/\partial\theta)(\phi, \theta)k,$$

$$\mathbf{T}_\phi = (\partial x/\partial\phi)(\phi, \theta)i + (\partial y/\partial\phi)(\phi, \theta)j + (\partial z/\partial\phi)(\phi, \theta)k. \tag{2, 3}$$

The 3D rotor geometry, which is shown in Figure 3, is defined by the discrete polar co-ordinates, R_m and θ_i, of one lobe, the length of the rotor L, and the wrap angle τ_m of the male rotor. Because of the symmetric geometry, the entire rotor can be easily defined. As a result, the total 3D surface can be completely defined using the integration variables θ and ϕ. The co-ordinates of the rotor surface S are defined in terms of θ and ϕ as

$$x(\phi, \theta) = R_m(\theta)\cos(\theta + \phi), \qquad y(\phi, \theta) = R_m(\theta)\sin(\theta + \phi), \qquad z(\phi, \theta) = (L/\tau_m)\phi. \tag{4–6}$$

Using this mapping scheme, the resulting integrations for the compression loads are

$$F_x = -\frac{PL}{\tau_m}\iint\left[\frac{\mathrm{d}R_m}{\mathrm{d}\theta}\sin(\theta + \phi) + R_m\cos(\theta + \phi)\right]\mathrm{d}\phi\ \mathrm{d}\theta, \tag{7}$$

$$F_y = \frac{PL}{\tau_m}\iint\left[\frac{\mathrm{d}R_m}{\mathrm{d}\theta}\cos(\theta + \phi) - R_m\sin(\theta + \phi)\right]\mathrm{d}\phi\ \mathrm{d}\theta, \tag{8}$$

$$F_z = -P\iint\frac{\mathrm{d}R_m}{\mathrm{d}\theta}R_m\,\mathrm{d}\phi\ \mathrm{d}\theta, \tag{9}$$

$$M_x = -P\iint\frac{\mathrm{d}R_m}{\mathrm{d}\theta}R_m^2\sin(\theta + \phi)\,\mathrm{d}\phi\ \mathrm{d}\theta - P\left(\frac{L}{\tau_m}\right)^2 \times \iint\left[\frac{\mathrm{d}R_m}{\mathrm{d}\theta}\cos(\theta + \phi) - R_m\sin(\theta + \phi)\right]\phi\ \mathrm{d}\phi\ \mathrm{d}\theta, \tag{10}$$

$$M_y = P \iint \frac{\mathrm{d}R_m}{\mathrm{d}\theta} R_m^2 \cos(\theta + \phi)\, \mathrm{d}\phi\, \mathrm{d}\theta - P\left(\frac{L}{\tau_m}\right)^2$$

$$\times \iiint \left[\frac{\mathrm{d}R_m}{\mathrm{d}\theta} \sin(\theta + \phi) + R_m \cos(\theta + \phi)\right]\phi\, \mathrm{d}\phi\, \mathrm{d}\theta, \tag{11}$$

$$M_z = PL/\tau_m \iint \frac{\mathrm{d}R_m}{\mathrm{d}\theta} R_m\, \mathrm{d}\phi\, \mathrm{d}\theta. \tag{12}$$

Now, the compression load computation is converted to a problem of double integration. However, the integration limits must be determined before implementation of the integration.

The integration limits are defined by the boundaries of the chamber being integrated. The limits on θ are simply the polar co-ordinates of adjacent lobe tips on the 2D profile. The limits on ϕ are defined by the suction and discharge planes and interlobe seal curve. For the integration they are defined by the end points of the helical lines associated with the discrete polar co-ordinates. These limits are directly related to the z co-ordinates of the boundaries by

$$z = (L/\tau_m)\phi. \tag{13}$$

If a specific helical line does not intersect the interlobe seal curve, the endpoints of the line are the suction and discharge planes. These endpoints occur at $z = 0$ and $z = -L$, corresponding to limits of $\phi = 0$ and $\phi = \tau_m$, respectively.

If a specific helical line intersects the interlobe seal curve, the section is divided into two chambers. Separate integrations are implemented for the variable ϕ, which is a function of θ. For the intake chamber, the limits are from zero to the seal line. For the compression chamber, the limits are from the seal line to the wrap angle τ_m. The seal data are so defined that each point on the 2D rotor profile corresponds to a specific reference seal point. Therefore, the limits on ϕ can be determined for each value of θ. The compression loads for the entire rotor at the specific incremental value θ_m, are the summation of the integrals for each helical section.

In the work by Adams and Soedel [5], a forward difference is used for the approximation of the derivative $\mathrm{d}R/\mathrm{d}\theta$ contained in equations (7)–(12). However, a central difference formula is adopted here to improve the accuracy of the evaluation. The value $\mathrm{d}R/\mathrm{d}\theta$ can be written as

$$\left.\frac{\mathrm{d}R}{\mathrm{d}\theta}\right|_{\theta=\theta_i} = R(\theta_{i-1}) \frac{\theta_i - \theta_{i+1}}{(\theta_{i-1} - \theta_i)(\theta_{i-1} - \theta_{i+1})} + R(\theta_i) \frac{2\theta_i - \theta_{i-1} - \theta_{i+1}}{(\theta_i - \theta_{i-1})(\theta_i - \theta_{i+1})}$$

$$+ R(\theta_{i+1}) \frac{\theta_i - \theta_{i-1}}{(\theta_{i+1} - \theta_{i-1})(\theta_{i+1} - \theta_i)}. \tag{14}$$

Making use of profile symmetry, at the beginning point $i = 1$, θ_0 is replaced with $\theta_n - 2\pi/N_m$, and at the end point $i = n$, θ_{n+1} is replaced with $\theta_1 + 2\pi/N_m$. For equations (7), (8), (10) and (11), the integration formula can be expressed as

$$I_1 = \int_{\theta_0}^{\theta_n} \int_{a(\theta)}^{b(\theta)} f(\theta, \phi)\, \mathrm{d}\phi\, \mathrm{d}\theta. \tag{15}$$

Because of the unevenly spaced tabulated data of the rotor profile, the composite trapezoid method is adopted. One can derive the routine for this kind of integration as

$$I_1 = \frac{1}{4m}\,[(b(\theta_0) - a(\theta_0))\,(f(\theta_0, a(\theta_0)) + 2\sum_{k=1}^{m-1} f(\theta_0, \phi_k\,(\theta_0) + f(\theta_0, b(\theta_0)))\,(\theta_1 - \theta_0)$$

$$+ \sum_{i=1}^{n-1} [b(\theta_i) - a(\theta_i))\,(f(\theta_i, a(\theta_i)) + 2\sum_{k=1}^{m-1} f(\theta_i, \phi_k\,(\theta_i))$$

$$+ f(\theta_i, b(\theta_i)))\,(\theta_{i+1} - \theta_{i-1}) + [(b(\theta_n) - a(\theta_n))\,(f(\theta_n, a(\theta_n))$$

$$+ 2\sum_{k=1}^{m-1} f(\theta_n, \phi_k\,(\theta_n) + f(\theta_n, b(\theta_n)))\,(\theta_n - \theta_{n-1})], \tag{16}$$

where

$$\phi_k = a(\theta) + k(b(\theta) - a(\theta))/m. \tag{17}$$

For equations (9) and (12), the integration form can be expressed as

$$I_2 = \int_{\theta_0}^{\theta_n} \int_{a(\theta)}^{b(\theta)} f(\theta)\,\mathrm{d}\phi\,\mathrm{d}\theta. \tag{18}$$

In a similar way, one can perform the integration to get the formula

$$I_2 = \tfrac{1}{2}\,[(b(\theta_0) - a(\theta_0))\,f(\theta_0)\,(\theta_1 - \theta_0) + \sum_{i=1}^{n-1} (b(\theta_i) - a(\theta_i))\,f(\theta_i)\,(\theta_{i+1} - \theta_{i-1})$$

$$+ (b(\theta_n) - a(\theta_n))\,f(\theta_n)\,(\theta_n - \theta_{n-1})]. \tag{19}$$

These integrals are used to compute forces and moments corresponding to the given co-ordinate system whose origin is located at the center of the rotor on the suction plane. Moreover, these loads can be resolved to forces at the suction and discharge bearings and moments about the axis of rotation for each rotor by assuming simple supports at the bearings.

A computing program has been developed for the calculation of the compression loads. This program can be used to calculate the compression loads for various rotor profiles. The program reads the geometrical data files given by the user and, after the calculation, outputs the results in the form of forces in the x, y, z directions and moments about x-, y-, z-axes for each rotor or in the form of suction and discharge bearing forces and moments for each rotor. Using this scheme, the compression loads are sensitive to the spacing between the profile data points. Special attention must be paid to the definition of the integration regions, especially in the regions where variation in the profile radius with respect to θ_i is the greatest [6].

A specific compressor configuration is defined as the working model and used to demonstrate the capability of the algorithms and program. Its main geometrical parameters are lobes combination (N_m /N_f): 6/7; rotor length: 96 mm; wrap angle: 3·7385 rad.

The geometrical data for the profile and seal line is given by tabulated data in terms of the angular co-ordinate θ_i. The operating conditions are assumed as port timing: $\theta_{spc} = 427^\circ$, $\theta_{dpo} = 488^\circ$; under-pressure running condition: $P_{suc} = 310$ Kpa (45 psi), $P_{dis} = 1048$ Kpa (152 psi).

The calculated results from equations (7)–(12) are presented in Figure 4. It should be mentioned that the compression loads obtained are applied to the rotor centers of the suction planes for both the male and female rotors. It can be seen from the charts that the compression loads are periodic functions with respect to the male rotor angle θ_m due to the symmetry of the rotor. Assuming the male rotor rotates at constant speed, the compression loads vary periodically with time. In addition, the moment about the axis of rotation M_z for the male rotor is much larger than that for the female rotor, which functions nearly as an idler.

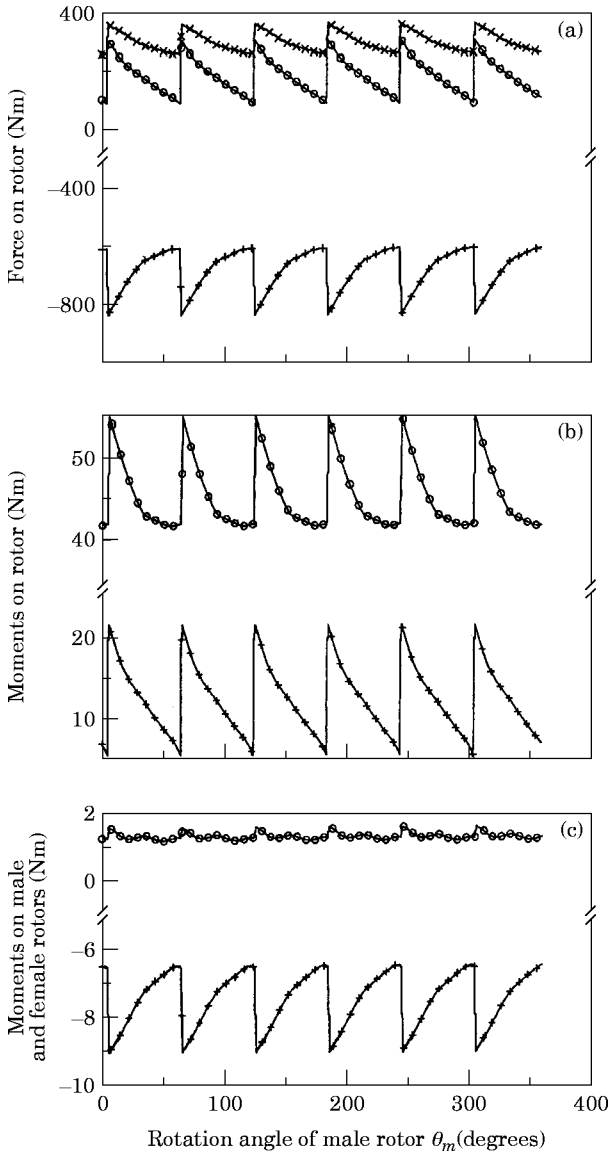

Figure 4. (a) Forces on the male rotor in the x, y, z directions: —+—, F_x ; —○—, F_y ; — × —, F_z ; (b) moments on the male rotor about the x- and y-axes: —+—, M_x ; —○—, M_y ; (c) moments on the male and female rotors about the z-axis: —+—, M_{zm} ; —○—, M_{zf}.

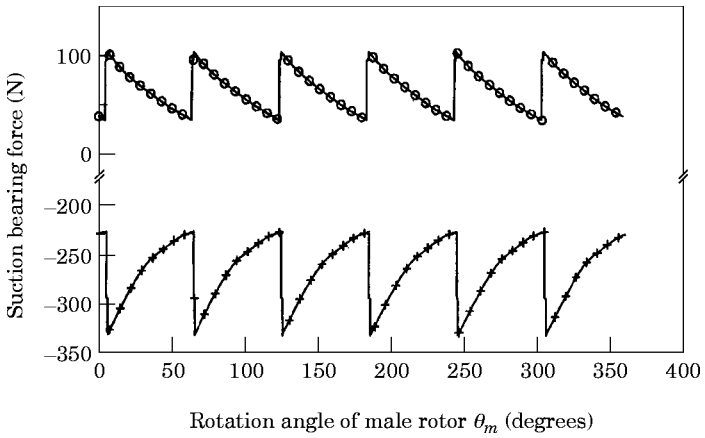

Figure 5. Suction bearing forces of the male rotor in the x and y directions: —+—, R_{sx}, —○—, R_{sy}.

The compression loads on the rotors can be resolved to the bearing forces by assuming the boundary conditions at the bearings as ideal, simple supports. The suction bearing loads with ideal boundary conditions are presented in Figure 5. It will be seen in the next section that the bearing loads will be different if the rotor motion and bearing stiffness are taken into consideration.

3. SCREW COMPRESSOR MODEL

Typically, the screw compressor rotors and the supported bearings form a rotor bearing system. The loads on the rotor are transferred to the bearings while the rotor is rotating. It is necessary to study the behavior of the bearings so that the load transmission can be more accurately described.

Based on the concept of Hertzian contact stress [7, 16], the load deflection relationships for a single rolling element can be expressed as

$$Q_j = K\delta_j^n, \tag{20}$$

where Q_j is the normal load on the ball or roller, δ_j is the normal contact deformation, K is the deflection constant and n is equal to 3/2 for ball bearings with point contact and 10/9 for roller bearings with line contact.

Harris [16] also gives the formulas for computing the deflection constant K. For steel ball-steel raceway contact, K values of the ball-inner raceway and ball-outer raceway contact are

$$K_{i,o} = 2{\cdot}15 \times 10^5 \left(\sum \rho_{i,o} \right)^{-1/2} (\delta_{i,o}^*)^{-3/2}. \tag{21}$$

Similarly, for steel roller and raceway contact,

$$K_{i,o} = 7{\cdot}86 \times 10^4 l^{8/9}. \tag{22}$$

Finally, the combined deflection constant for bearings is

$$K = (1/[(1/K_i)^{1/n} + (1/K_o)^{1/n}])^n, \tag{23}$$

where K_i is the deflection constant for inner raceway, K_o is for outer raceway and K is for either ball bearings ($n = 3/2$) or roller bearings ($n = 10/9$).

Generally, it is assumed that the outer raceway is fixed in the bearing housing and the inner raceway is attached to the rotor. The inner raceway is subjected to displacements of five degrees of freedom x, y, z, θ, ϕ, with respect to the outer raceway. The resulting interacting forces and moments f_x, f_y, f_z, m_x, m_y are shown in Figure 6. For a ball bearing, the deflection of the ball can be expressed as

$$\delta_{bj} = \begin{cases} A_j - A, & \delta_{bj} > 0, \\ 0, & \delta_{bj} \leqslant 0, \end{cases} \tag{24}$$

where

$$A_j = ((A \sin \alpha_0 + \delta_{zj})^2 + (A \cos \alpha_0 + \delta_{rj})^2)^{1/2} \tag{25}$$

and where A is the unloaded relative distance between the inner and outer raceway groove curvature center and A_j is the loaded relative distance.

The deflection of the jth ball in the axial δ_{zj} and radial δ_{rj} can be obtained from the relationships shown in Figure 7:

$$\delta_{zj} = z + r_j (\theta \sin \psi_j - \phi \cos \psi_j), \qquad \delta_{rj} = x \cos \psi_j + y \sin \psi_j - r_c. \tag{26, 27}$$

In equation (26), r_j is the radius of the locus of the centers of the inner raceway groove curvature. It can be written as

$$r_j = \tfrac{1}{2} d_m + (r_i - 0{\cdot}5D) \cos \alpha_j. \tag{28}$$

With the above deflection, the contact angle is changed. It can be expressed as

$$\tan \alpha_j = (A \sin \alpha_0 + \delta_{zj})/(A \cos \alpha_0 + \delta_{rj}). \tag{29}$$

It is assumed that the relative angular position of each rolling element is always maintained due to rigid cages and pin retainers. Centrifugal forces and gyroscopic moments on the

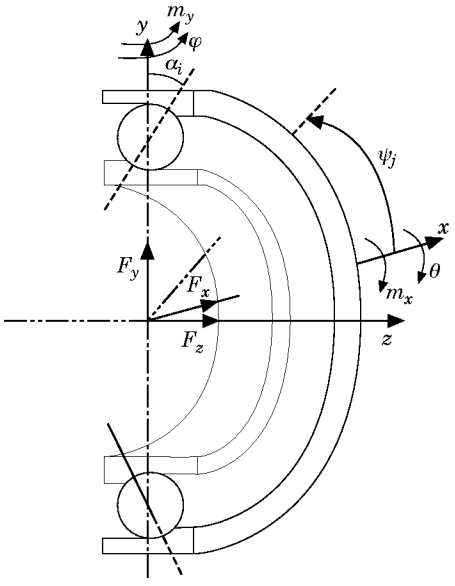

Figure 6. Five-degrees-of-freedom model of the rolling bearing.

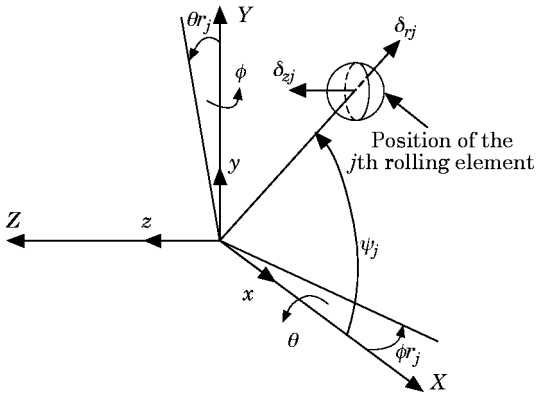

Figure 7. Relationships of δ_{zj} and δ_{rj} with the displacements of the inner raceway.

bearing are ignored because of comparatively low rotational speeds of the rotor. The interacting forces and moments can be expressed as

$$B_x = \sum_j^z K(\delta_{bj})^{3/2}(-\cos\alpha_j \cos\psi_j), \qquad B_y = \sum_j^z K(\delta_{bj})^{3/2}(-\cos\alpha_j \sin\psi_j),$$

$$B_z = \sum_j^z K(\delta_{bj})^{3/2}(-\sin\alpha_j), \tag{30–32}$$

$$M_{bx} = \sum_j^z r_j K(\delta_{bj})^{3/2}(-\sin\alpha_j \sin\psi_j), \qquad M_{by} = \sum_j^z r_j K(\delta_{bj})^{3/2}(\sin\alpha_j \cos\psi_j), \tag{33, 34}$$

where z is the number of balls of the bearing.

In all of the above equations, ψ_j refers to the relative position of the jth ball with respect to the x-axis. When the bearing is under operation, ψ_j is a function of time t:

$$\psi_j = (2\pi/z)j + \omega_c t, \tag{35}$$

where ω_c is the cage angular velocity. For slow speed rotation with the outer raceway fixed, if it is assumed that there is no gross slip at the raceway contact, the angular speed of the cage relative to the inner raceway is [16]

$$\omega_c = \tfrac{1}{2}\,\Omega(1 - D\cos\alpha_j/d_m), \tag{36}$$

where Ω is the angular speed of the rotor.

Now consider a cylindrical roller bearing and ignore the misalignment of the roller bearing. The deflection for the jth roller can be expressed as

$$\delta_{Rj} = \delta_{rj} = x\cos\psi_j + y\sin\psi_j - r_c. \tag{37}$$

In a similar way as for the ball bearing, the interacting forces can be expressed as

$$R_x = \sum_j^z K(\delta_{Rj})^{10/9}(-\cos\psi_j), \qquad R_y = \sum_j^z K(\delta_{Rj})^{10/9}(-\sin\psi_j). \tag{38, 39}$$

Equations (35) and (36) for the ψ_j and ω_c calculation are also valid for the roller bearing, but in equation (36), α_j is equal to zero for the cylindrical roller bearing.

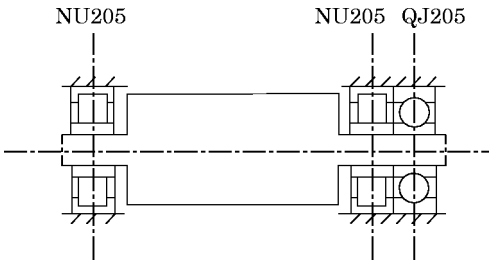

Figure 8. A typical screw compressor system model.

It should be mentioned that similar expressions with minor differences for the interactions between the rotor and bearings have also been used for different purposes by Jones [7], Lim and Singh [15], Harris [16] and Eschmann *et al*. [17].

In Figure 8, the screw compressor system model consists of a rotor supported by a pair of cylindrical roller bearings NU205, which is the radial load, and a four point contact ball bearing QJ205, which is mainly for the axial load. There are five degrees of freedom as shown in Figure 9. They are the radial directions x and y in the vertical plane x–y, the axial direction z, and the rotation motions θ about the x-axis and ϕ about the y-axis. The origin of the co-ordinate system is at the gravity center of the rotor. The x-axis is directed from the center of the male rotor to the female rotor. The z-axis is directed from the discharge plane to the suction plane. Once the displacements of the gravity center of the rotor are determined, the displacements at any points on the rotor can be then obtained by the geometric relations of the rotor.

To set up a mathematical model for the system, it is assumed that the rotor is rigid. The natural modes due to the rotor flexibility are not considered. The body force of the rotor due to gravity is neglected due to its magnitude compared with the compression loads. Also, the load deflection relation for each elastic rolling element is assumed to be defined by the Hertzian contact theory and the load experienced by each rolling element is described by its relative location in the bearing raceway. The effect of the elastohydrodynamic film is ignored. Further, the rolling elements in the bearings are assumed to be equally positioned during their operation due to rigid cages and pin retainers. The centrifugal and gyroscopic effects of the rolling elements are neglected as these effects are evident only at extremely high operating speeds [18]. The torsional vibration of the rotor is also ignored since it is beyond the scope of this study.

Figure 9 is the free body diagram for the system in Figure 8. The interacting loads at the left cylindrical roller bearing NU205 are represented as R_{sx}, R_{sy} and at the right cylindrical roller bearing NU205 as R_{dx}, R_{dy}. The interacting loads for the four point contact ball bearing QJ205 are denoted as B_x, B_y, B_z, M_{bx}, M_{by}. The rotor is subjected

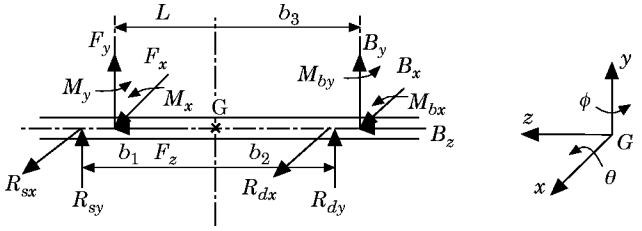

Figure 9. Free body diagram for the screw compressor model.

to a set of external compression loads F_x, F_y, F_z, M_x, M_y as computed in the previous section.

From the free body diagram, by applying Euler's equations of motion for rigid bodies and assuming a constant operating speed Ω, the governing equations of the rotor bearing system can be expressed as

$$M\,\mathrm{d}^2x/\mathrm{d}t^2 = F_x + B_x + R_{sx} + R_{dx}, \qquad M\,\mathrm{d}^2y/\mathrm{d}t^2 = F_y + B_y + R_{sy} + R_{dy},$$

$$M\,\mathrm{d}^2z/\mathrm{d}t^2 = F_z + B_z, \tag{40–42}$$

$$I\,\mathrm{d}^2\theta/\mathrm{d}t^2 + I_z\,\Omega\,\mathrm{d}\phi/\mathrm{d}t = -F_y\,L + B_y\,b_3 - R_{sy}\,b_1 + R_{dy}\,b_2 + M_x + M_{bx}, \tag{43}$$

$$I\,\mathrm{d}^2\phi/\mathrm{d}t^2 - I_z\,\Omega\,\mathrm{d}\theta/\mathrm{d}t = F_x\,L - B_x\,b_3 + R_{sx}\,b_1 - R_{dx}\,b_2 + M_y + M_{by}, \tag{44}$$

The interactions between the rotor and bearings in the above equations can be determined by the methods illustrated in the previous sections. Therefore, there are five unknowns to be solved. These unknowns x, y, z, θ and ϕ are the displacements in the x, y and z directions and angular displacements about the x- and y-axes, respectively.

In the rotor bearing system, the choice of initial conditions is immaterial as the steady state solution is reached with a limit cycle vibration which is independent of the initial conditions [14]. Therefore, the initial conditions are assumed to be

$$x = y = z = \theta = \phi = 0. \tag{45}$$

It should be noted that, in the above equations, the interactions between the rotor and bearings are functions of the displacements x, y, z, θ and ϕ. Therefore, these equations are non-linear second order ordinary differential equations. An effective way to solve these equations of motion for the system is presented.

A computer program has been written to solve the equations of motion for the specific configuration in Figure 10. The average acceleration method [19] is employed to obtain velocity and displacement components. The calculation procedure is as follows:

(1) Input the bearing geometry, rotor geometry, rotor rotational speed and excitation loads.

(2) Set the initial conditions at $t = 0$, and from equations (40)–(44) calculate the accelerations

$$\ddot{x}_0, \ddot{y}_0, \ddot{z}_0, \ddot{\theta}_0, \ddot{\phi}_0.$$

(3) Applying the average acceleration method, find the variables

$$(\dot{x}_i)_j, (\dot{y}_i)_j, (\dot{z}_i)_j, (\dot{\theta}_i)_j, (\dot{\phi}_i)_j, (x_i)_j, (y_i)_j, (z_i)_j, (\theta_i)_j, (\phi_i)_j,$$

where j is the iteration counter within the ith time step.

(4) From the above obtained values which represent the displacements of the rotor gravity center, calculate the corresponding displacements at the supporting bearings. For the suction roller bearing,

$$x_s = x + b_1\,\phi, \qquad y_s = y - b_1\,\theta. \tag{46}$$

For the discharge roller bearing,

$$x_d = x - b_2\,\phi, \qquad y_d = y + b_2\,\theta. \tag{47}$$

For the ball bearing,

$$x_b = x - b_3\,\phi, \qquad y_b = y + b_3\,\theta. \tag{48}$$

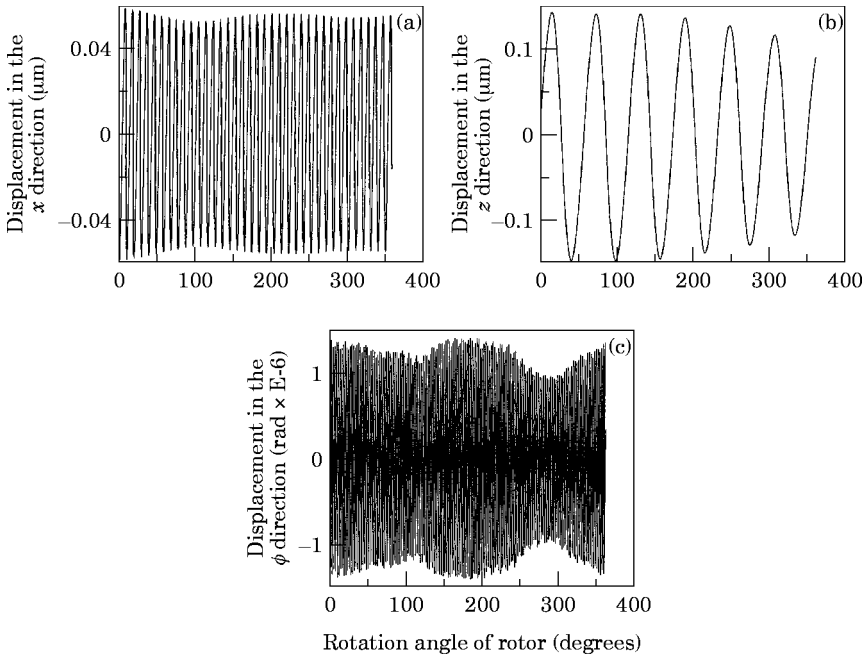

Figure 10. (a) Response of rotor gravity center in the x direction, (b) response of rotor gravity center in the z direction, (c) response of rotor gravity center in the ϕ direction.

The z direction displacement for all the bearings are the same as the z displacement for the rotor gravity center.

(5) Determine the dynamic contact angle α_j and the deflection δ_j according to the corresponding displacement at the bearings from equations (29), (24) and (37).

(6) Compute the interactions between the rotor and bearings from the equations (26)–(34) and (38, 39).

(7) Substitute the interactions into equations (40)–(44) to get the values of $\ddot{x}$, $\ddot{y}$, $\ddot{z}$, $\ddot{\theta}$, $\ddot{\phi}$.

(8) Examine the convergence criterion for the iterative procedure within each time step. In this analysis, the following criterion is adopted:

$$\frac{|(x, y, z, \theta, \phi)_{i,j} - (x, y, z, \theta, \phi)_{i,j-1}|}{|(x, y, z, \theta, \phi)_{i,j}|} \leqslant \varepsilon, \tag{49}$$

where ε is normally takes as 0·01–0·001. If the criterion given by equation (49) is not satisfied, return to step (3) and repeat the procedure. If the criterion is satisfied, proceed to the next time station and start from step (3).

By adopting the procedure illustrated above, the displacements of the rotor gravity center x, y, z, θ, ϕ as functions of rotation angle of the male rotor or the time sequence can be determined. In addition, the interactions of roller and ball bearings with the rotor can be obtained. All of these interactions are also functions of rotation angle of the male rotor or the time sequence.

Table 1 shows the geometric parameters of the bearings which are used in the compressor configuration. Table 2 illustrates the parameters of the compressor male rotor. It should be noted that the model is oriented to simulate the dynamic performance for a specific configuration, in which the rotor is supported by two cylindrical roller bearings and a four point contact ball bearing. In can be also be used to model other configurations

TABLE 1

Parameters of the bearings

Parameters of the bearings	Cylindrical roller bearing	Four point contact ball bearing
Inner race bore D_i (mm)	22	25
Outer race outside diameter D_o (mm)	52	52
Bearing width B (mm)	15	15
Inner raceway diameter d_i (mm)	31·5	31·01
Outer raceway diameter d_o (mm)	46·5	46·94
Roller/ball diameter D (mm)	6·5	7·94
Number of roller/balls z	12	13
Roller effective length l (mm)	6·5	–
Inner groove radius r_i (mm)	–	4·015
Outer groove radius r_o (mm)	–	4·015
Pitch diameter of roller/ball set d_m (mm)	39	38·98
Unloaded contact angle α_o°	–	35

as well, such as the configuration in which the rotor is supported by two cylindrical roller bearings and a pair of tapered roller bearings. Only the interactions between the rotor and bearings have to be revised.

Figure 10 shows a set of simulation results of the rotor gravity center response as functions of the male rotor rotation angle under a set of impulse excitations. The rotor rotation speed is assumed to be constant at $\Omega = 3600$ r.p.m. Therefore, these results can also be taken as the rotor gravity center time history. Once the five displacements of the rotor gravity center are obtained, the displacements at any point on the rotor can be computed from the results by geometric relations.

The rotor is assumed to commence at

$$x = y = z = \theta = \phi = 0 \tag{50}$$

and to be operated under the conditions listed in Table 3. The excitations are applied to the rotor center at the suction plane.

From Figure 10, one can see that the response of the x displacement involves high vibration frequencies because the bearings have fairly high stiffness. The response of the ϕ displacement has even higher vibration frequencies since the ϕ displacement involves the frequencies created due to not only the bearing stiffness but also the gyroscopic effects of the rotor. It will be shown later that the two dominant frequencies of the ϕ displacement are related to both the bearing parameters and the mass moment of inertia of the rotor.

TABLE 2

Parameters of the compressor male rotor

Particulars of the male rotor	Values
Mass of the male rotor (kg)	2·138
Moment of inertia about the x–y-axis (kgm^2)	0·000441
Moment of inertia about the z-axis (kgm^2)	0·000010
Length of the male rotor (mm)	96
Distance from the C.G. to the suction roller bearing (mm)	79·5
Distance from the C.G. to the discharge roller bearing (mm)	72
Distance from the C.G. to the four point contact ball bearing (mm)	87

TABLE 3

Impulse excitations for the rotor bearing system

Impulse excitations to the rotor center at the suction plane	Values
Force in the x direction (N)	−612.24
Force in the y direction (N)	101.03
Force in the z direction (N)	255.80
Moment about the x-axis (Nm)	6.77
Moment about the y-axis (Nm)	41.67

The response of the z displacement has comparatively lower frequency than any other responses. This is because the z direction vibration depends mostly on the axial stiffness of the ball bearings. The axial stiffness of the four point contact ball bearing is lower than the radial stiffness of the roller bearings. Therefore, it exhibits a lower frequency response in the z direction. The phenomena can be seen clearly in the frequency spectra.

Figure 11 shows the x–y locus of the rotor gravity center under the same impulse excitations. The basic shape of the orbit is an ellipse because of the different magnitudes of the forces in the x and y directions. This agrees qualitatively with the results of studies by Rehnejat and Gohar [20] and Aini *et al*. [14]. The ellipse whirls at a certain speed around a certain point. The whirling direction is the same as the direction of the rotor rotation. Rao [8] presented similar phenomenon when he studied the out-of-balance responses of rotors on fluid film bearings.

A set of frequency spectra for the response in Figure 10 under the impulse excitations are obtained using a Fast Fourier Transformation, which are shown in Figure 12. They indicate the same frequency characteristics as stated previously. The frequency spectrum of the x displacements displays a dominant frequency f_b of approximate 2280 Hz, which is related to the roller bearings. The frequency response of the z direction has a dominant frequency f_z of about 420 Hz, which is related to the ball bearing. The frequency spectrum of the ϕ displacement has two dominant frequencies. The lower one which has the same values as f_b is related to the roller bearings. The higher frequency f_i is related to the roller bearings as well as the moment of inertia of the rotor about the x- or y-axes. The other two distinct frequencies f_1 and f_2 in the ϕ spectrum are combinations of f_b and f_i. The

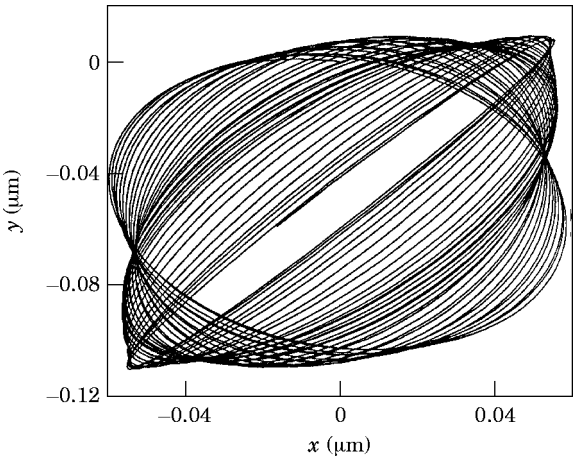

Figure 11. Locus of rotor gravity center in the x–y plane.

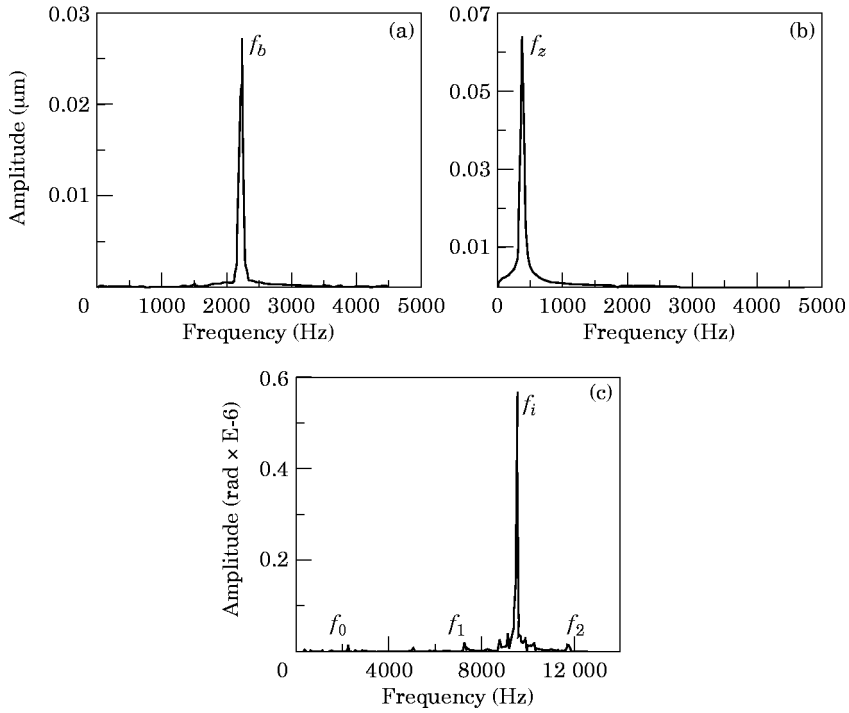

Figure 12. (a) Frequency spectrum of the (a) x displacement, (b) z displacement and (c) ϕ displacement under impulse excitations.

frequency f_1 is approximately equal to $f_i - f_b$ and the frequency f_2 is equal to $f_i + f_b$. The response of the y displacement is similar to that of the x displacement and the response of the θ to that of the ϕ.

All of the above dominant frequencies in the frequency spectra are related to the parameters of the rotor bearings system. By varying some of the parameters of the system and observing the frequency response variation, we can investigate how the values of the dominant frequencies will change correspondingly. It is useful to study the effects of the parameters on the system responses for providing a critique of the compressor design.

The effects of parameters of the rotor and bearings on the system responses can be studied upon the application of the impulse excitations. Figure 13 shows how the

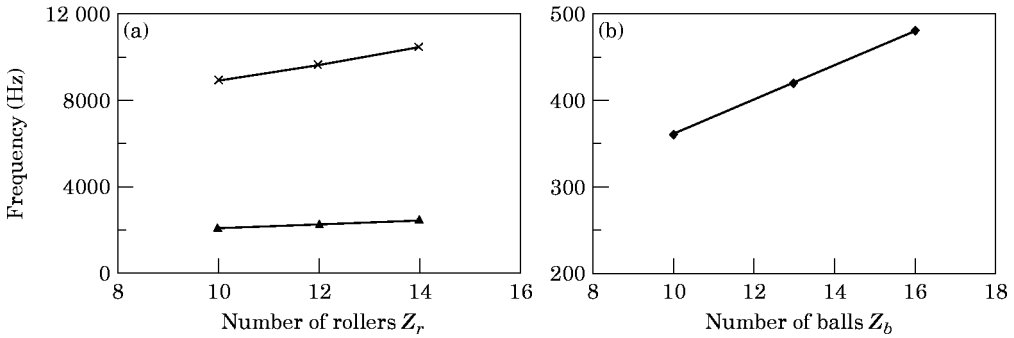

Figure 13. (a) Effects of numbers of rollers on the frequencies: —▲—, f_b ; —×—, f_i ; (b) effects of number of balls on the frequencies f_z.

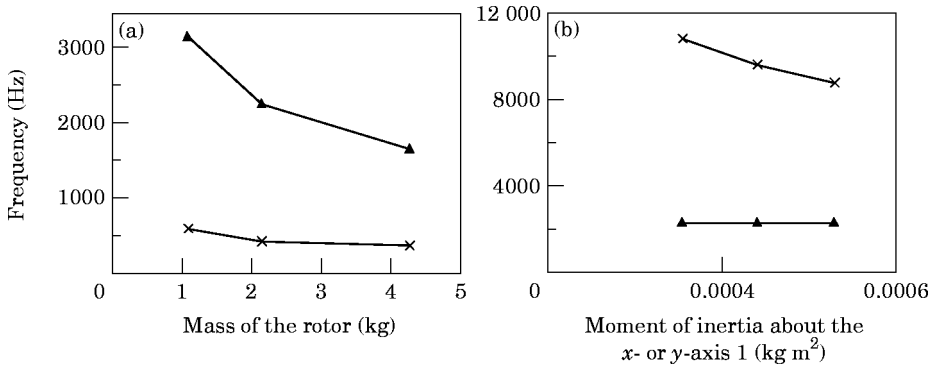

Figure 14. (a) Effects of rotor mass on the frequencies —▲—, f_b and —×—, f_z; (b) effects of moment of inertia I on the frequencies —▲—, f_b and —×—, f_i.

frequencies f_b and f_i vary with the changes of the number of rollers in the roller bearings. The greater number of rollers results in larger dominant frequencies because of the higher stiffness of the roller bearings. However, it is found that the frequency f_z remains unchanged as the number of rollers increases. This is because f_z is the dominant frequency of vibration in the axial direction and the roller bearings mainly support the radial loads. Actually, f_z does vary with the number of balls in the four point contact ball bearing while f_b and f_i reamin unchanged. This indicates that the ball bearing mainly supports the axial load and has little effect on the responses in the radial directions.

Figure 14 shows the effects of the rotor mass on the dominant frequencies. It can be seen that f_b and f_z decrease as the mass of the rotor increases, whereas f_i has no significant change and is not shown. It is found that the moment of inertia about the x- or y-axis has little effect on the frequencies f_b, but f_i varies with the change of the moment of inertia correspondingly. This indicates that f_b is the frequency related to the transverse vibration whereas f_i is related to the rocking vibration of the rotor.

The compression loads which were computed in the previous section are applied to the rotor. The responses of the suction bearing forces are presented in Figure 15 under an operating speed of 3600 r.p.m. for the screw compressor configuration shown in Figure 8.

Figure 15 shows that the bearing forces in the screw compressor involve very high frequencies when the model couples the rotor motion with the bearing stiffness as

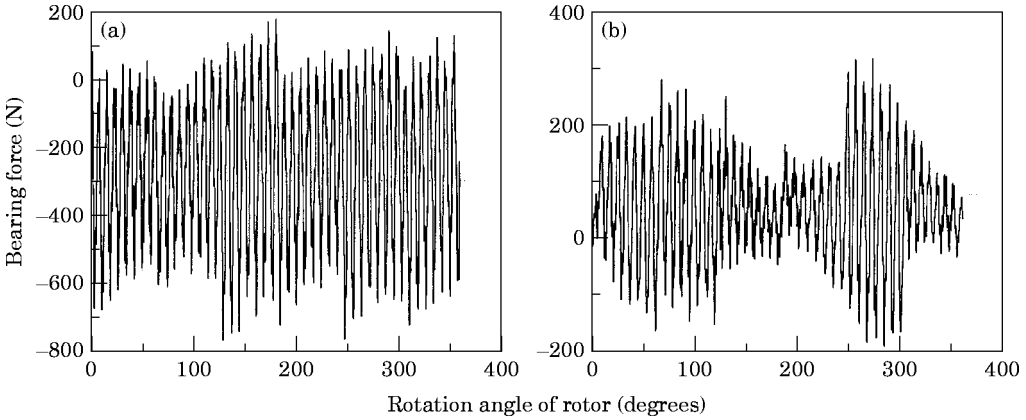

Figure 15. (a) Suction roller bearing force in the x direction, (b) suction roller bearing force in the y direction.

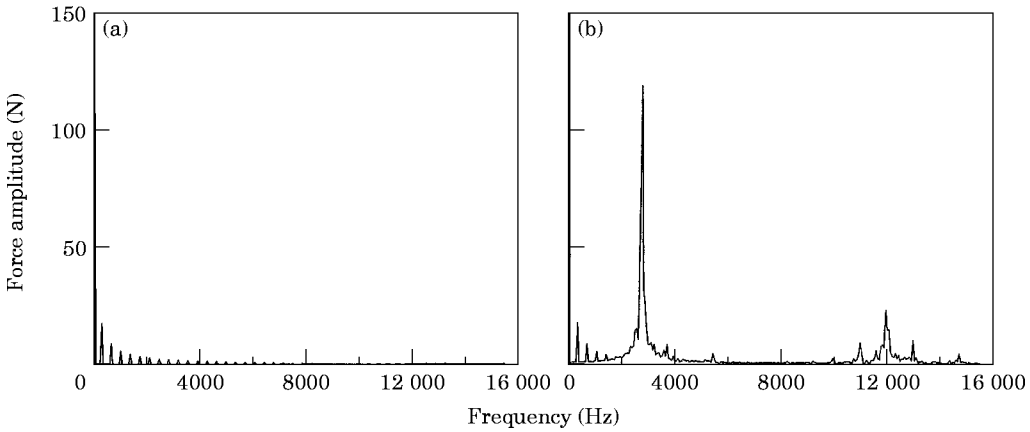

Figure 16. Frequency spectrum of the suction bearing force in the x direction by (a) assuming ideal boundary conditions, (b) by coupling the rotor motion and bearing stiffness.

compared with the bearing forces obtained by assuming ideal, simply supported boundary conditions at the bearings. It should be noted that envelope shapes of the bearing force responses are similar to the shapes of the bearing force responses with ideal boundary conditions. The shapes of the bearing force responses in both cases follow the shapes of the compression loads on the rotor which have been shown in Figure 4. With the same operating condition, the maximum values of the bearing forces are higher than those computed in the last section. For example, the maximum value of the suction end bearing force in the x direction in Figure 15 is approximately two times greater than in Figure 5.

Figure 16 shows the comparison of the frequency spectrum of the suction bearing force in the x direction by assuming ideal boundary conditions with that when coupling the rotor motion and bearing stiffness. When assuming ideal boundary conditions, the frequency spectrum of the bearing force directly reflects the frequency characteristics of the compression force. However, when coupling the rotor motion and bearing stiffness, the frequency spectrum of the bearing force includes the frequency characteristics of the compression force in the lower frequency range, below 2000 Hz, and exhibits the frequency characteristics of the rotor bearing system in the higher frequency range. By including the rotor dynamics in the bearing force computation, the bearing forces are expected to reflect the dynamic behavior of the bearings in the screw compressor more accurately.

The bearing forces for the female rotor can be obtained by the same model and procedure with only some revision needed of the parameters of the rotor and with different excitations from the compression loads.

4. CONCLUSIONS

A method for the computation of compression loads in a twin screw compressor is provided using vector calculus and numerical integration. A computer program based on this method is developed for computing the compression loads. Thus, a robust procedure which can be applied to arbitrary rotor profiles and various operating conditions has been developed. These computations are useful in obtaining forcing input for simulating dynamics of the rotors during operation.

The method for the computation of compression loads developed in the previous work employed forward difference formulation in computing the numerical integrations. The current method improves the algorithm by employing the central difference formulations

for the approximation of the derivative of the profile radius with respect to the angular co-ordinate $dR/d\theta$, and by using the composite trapezoid integration method.

A dynamic model for the rotor bearing system in the screw compressor is developed from basic principles. This model includes a rigid rotor of five degrees of freedom supported by two cylindrical roller bearings and a four point contact ball bearing. It couples the global rotor motion with the local dynamics of the bearings having non-linear characteristics. It can be used to obtain the system responses and study the dynamic performance of the screw compressor under various operating conditions.

By analysis of the frequency spectra, the effects of certain parameters of the rotor and the bearings on the system responses are studied. Analysis shows that the dominant frequencies of the system responses are affected by the number of rollers and balls, the rotor mass and the moment of inertia of the rotor about the x- and y-axes. The relations between the parameters and the dominant frequencies are presented.

When the compression loads are applied to the rotor, the bearing forces are examined. In the previous work by You *et al*. [3], Adams and Soedel [5], and Qin and Adams [6], the bearing forces are computed by assuming ideal simply supported boundary conditions. In this work, the bearing forces are obtained by coupling the rotor motion with the bearing stiffness having non-linear behavior. The results are expected to be more reasonable and accurate. It has been shown that the shapes of the envelope of the bearing force responses are similar to those with ideal boundary conditions at the bearings but the magnitudes of the responses are higher than by assuming ideal boundary conditions at the bearings. In addition, the bearing force responses involve high frequencies due to the high stiffness at the bearings.

REFERENCES

1. G. P. Adams and W. Soedel 1994 *Proceedings of the* 1994 *International Compressor Engineering Conference at Purdue* (W. Soedel, editor) **I**, 67–72. A method for computing the compression loads in twin screw compressors.
2. Z. Zhou, D. Wang, T. Zhu and J. Mao 1990 *Proceedings of the* 1990 *International Compressor Engineering Conference at Purdue* (W. Soedel, editor) **I**, 8–17. Analysis of the applied forces in twin screw refrigeration compressors.
3. C. X. You, Y. Tang, J. S. Fleming and A. B. Tramschek 1994 *Proceedings of the* 1994 *International Compressor Engineering Conference at Purdue* (W. Soedel, editor) **II**, 653–658. A generalized computer program for calculating the bearing loads in helical twin screw compressors.
4. G. P. Adams and W. Soedel 1992 *Proceedings of the* 1992 *International Compressor Engineering Conference at Purude* (J. F. Hamilton, editor) pp. 439–477. Remarks on oscillating bearing loads in twin screw compressors.
5. G. P. Adams and W. Soedel 1995 *Transactions of the American Society of Mechanical Engineers*, *Journal of Mechanical Design* **117**, 512–519. Computation of compression loads in twin screw compressors.
6. Z. Qin and G. P. Adams 1996 *Proceedings of* 1996 *ASME International Mechanical Engineering Conference* **I**, 163–169. An approach for the calculation of compression loads in helical twin screw compressors.
7. A. B. Jones 1960 *Transactions of the American Society of Mechanical Engineers*, *Journal of Basic Engineering* **82**, 309–320. A general theory for elastically constrained ball and radial roller bearings under arbitrary load and speed conditions.
8. J. S. Rao 1983 *Rotor Dynamics*. New York: John Wiley.
9. H. N. Ozguven 1984 *Transactions of the American Society of Mechanical Engineers*, *Journal of Vibration*, *Acoustics*, *Stress and Reliability in Design* **106**, 59–61. On the critical speed of continuous shaft–disk systems.
10. A. Craggs 1993 *Transactions of the American Society of Mechanical Engineers*, *Journal of Sound and Vibration* **160**, 559–565. Effect of distributed bearing stiffness on the critical speeds of shafts.

11. V. R. Redddy and A. M. Sharan 1987 *Transactions of the American Society of Mechanical Engineers*, *Journal of Vibration*, *Acoustics*, *Stress and Reliability Design* **109**, 407–415. The finite element modelled design of lathe spindles: the static and dynamic analysis.
12. E. P. Gargiulo 1980 *Machine Design* 107–110. A simple way to estimate bearing stiffness.
13. C. H. Chen, K. W. Wang and Y. C. Shin 1994 *Transactions of the American Society of Mechanical Engineers*, *Journal of Vibration and Acoustics* **116**, 506–513. An integrated approach toward the dynamic analysis of high speed spindles, Part I: system model.
14. R. Aini, H. Rahnejat and R. Gohar 1990 *International Journal of Machine Tools Manufacture* **20**, 1–18. A five-degrees-of-freedom analysis of vibrations in precision spindles.
15. T. C. Lim and R. Singh 1990 *Transactions of the American Society of Mechanical Engineers*, *Journal of Sound and Vibration* **139**, 179–225. Vibration transmission through rolling element bearings, Part I: bearing stiffness formulation and part II: system studies.
16. T. A. Harris 1991 *Rolling Bearing Analysis* (third edition). New York: John Wiley.
17. P. Eschmann, L. Hasbargen and K. Weigand 1985 *Ball and Roller Bearings*. New York: John Wiley.
18. Y. C. Shin 1992 *Transactions of the American Society of Mechanical Engineers*, *Journal of Engineering for Industry*, **114**, 23–30.
19. S. Timoshenko, D. H. Young and W. Weaver 1974 *Vibration Problems in Engineering* (fourth edition). New York: John Wiley.
20. H. Rahnejat and R. Gohar 1985 *Proceedings of the Institution of Mechanical Engineering* **199**, C3, 181–193. The vibrations of radial ball bearings.

APPENDIX: LIST OF SYMBOLS

A	unloaded distance between the inner and outer raceway groove curvature centers
A_j	loaded distance between the inner and outer raceway groove curvature centers
$a(\theta)$	lower limit of integration about ϕ
B_x, B_y, B_z	interactions of force between rotor and ball bearing in the x, y, z directions
b_1, b_2, b_3	bearing positions relative to rotor gravity center
$b(\theta)$	upper limit of integration about ϕ
C	constant defined by polytropic process
D	integration region/diameter of rolling element
d_m	bearing pitch diameter
$f(\theta, \phi), f(\theta)$	integrand functions
F_x, F_y, F_z	x, y, z components of the rotor forces due to compression
I	moment of inertia about the x- or y-axis
I_z	moment of inertia about the z-axis
G	rotor geometry center
K	deflection constant of bearing
$K_{i,o}$	deflection constant of ball/roller-inner raceway and ball/roller outer raceway contact
L	length of rotors
l	effective contact length of roller bearing
M	mass of rotor
M_{bx}, M_{by}	interactions of moment between rotor and ball bearing about the x-, y-axes
M_z, M_y	moments about the x- and y-axes of the rotor
M_{zm}, M_{zf}	moments about the z-axis of the male and female rotors due to compression
N_m, N_f	number of lobes on male rotor and number of flutes on female rotor
n	the polytropic constant for the gas being compressed/rolling element load deflection exponent
P_d	diametral clearance of ball bearing
P	chamber pressure as a function of θ_m
P_{suc}, P_{dis}	suction and discharge pressures
Q_j	resultant normal load on the jth rolling element
R_{sx}, R_{sy}	interactions of force between rotor and suction roller bearing in the x, y directions
R_{dx}, R_{dy}	interactions of force between rotor and discharge roller bearing in the x, y directions
R_m	discrete radial coordinate of male profile
r_j	radii of inner raceway groove curvature centers
r_c	bearing radial clearance
$S(\phi, \theta)$	the surface definition
$\mathbf{T}_\phi$ and $\mathbf{T}_\theta$	surface tangent vectors

t	time	ϕ_k	discrete co-ordinate of variable ϕ
z	number of rolling elements of bearing	θ	integration variable associated with polar co-ordinates/rotation
α_0	unloaded bearing contact angle		displacement of rotor gravity
α_j	loaded, the jth rolling element contact angle		center about the x-axis
		θ_i	discrete polar co-ordinate of male profile
ε	limit of convergence		
δ_{bj}	deflection of the jth ball	θ_{spc}	angular position when suction portion closes
δ_{Rj}	deflection of the jth roller		
δ_{rj}	distance of the jth element in the radial direction	θ_{dpo}	angular position when discharge portion opens
δ_{zj}	distance of jth rolling element in the axial direction	θ_m	the rotation angle of male rotor
		τ_m	wrap angle of male rotor
δ^*	non-dimension value for ball-raceway contact deformation	Ω	rotor rotation angular speed
		ω_c	angular speed of cage relative to inner raceway
ϕ	integration variable associated with helical twist/rotation displacement of rotor gravity center about the y-axis	ψ_j	relative position of the jth rolling element with respect to the x-axis